Wetting and brazing of (HfTaZrNbTi)B2 and (HfTaZrNbTi)C High-Entropy Ceramics by AgCuTi filler

Open Ceramics 22 (2025) 100792

Contents lists available at ScienceDirect

Open Ceramics

journal homepage: www.sciencedirect.com/journal/open-ceramics

Wetting and brazing of $(HfTaZrNbTi)B_2$ and (HfTaZrNbTi)C High-Entropy Ceramics by AgCuTi filler

Naser Hosseini [a], Fabrizio Valenza [b], Zdeněk Chlup [c], Sofia Gambaro [b], Carla Malinverni [d], Valentina Casalegno [d], Alexandra Kovalčíková [e], Monika Tatarková [a], Ivo Dlouhý [c], Peter Tatarko [a,*]

[a] Institute of Inorganic Chemistry, Slovak Academy of Sciences, Dúbravská cesta 9, 845 36 Bratislava, Slovakia
[b] Institute of Condensed Matter Chemistry and Technologies for Energy - ICMATE, National Research Council –CNR, Via De Marini 6, 16149 Genoa, Italy
[c] Institute of Physics of Materials, Czech Academy of Sciences, Žižkova 22, 616 00 Brno, Czech Republic
[d] Politecnico di Torino, Department of Applied Science and Technology, Corso Duca degli Abruzzi 24, 10129 Torino, Italy
[e] Institute of Materials Research, Slovak Academy of Sciences, Watsonova 47, 04001 Košice, Slovakia

ARTICLE INFO

Keywords:
High-entropy ceramics
Wetting
Brazing
AgCuTi alloy

ABSTRACT

The wetting behaviour of $(HfTaZrNbTi)B_2$ high entropy boride (HEB) and (HfTaZrNbTi)C high-entropy carbide (HEC) with molten Cu and AgCuTi alloy was investigated via the sessile drop method under an Ar/H_2 atmosphere. Pure Cu exhibited non-reactive wetting with contact angles ~ 120° on HEB and ~ 126° on HEC. In contrast, AgCuTi alloy showed strong reactive wetting (contact angle ≤ 17°), primarily driven by reactive Ti. The reaction layer was notably thicker for the HEC/AgCuTi system. Due to the better wetting behaviour and high-temperature interactions with the ceramic substrates, AgCuTi alloy was employed as a filler to braze HEB and HEC using pressure-less Field Assisted Sintering Technique (FAST). The resulting joints demonstrated high apparent shear strength of 176 ± 39 MPa for HEC and 116 ± 38 MPa for HEB, exceeding the strength of the base materials in both cases.

1. Introduction

High-entropy boride (HEB) and carbide (HEC) ceramics, composed of transition metal elements, represent novel ultra-high temperature ceramics (UHTCs) with promising potential applications in the aerospace and nuclear energy industries. These materials have garnered significant attention due to their superior properties, such as high hardness, high elastic modulus, high strength, high fracture toughness, high thermal stability, and oxidation resistance when compared to conventional binary carbides and borides [1–3]. The pioneering development of boride [4] and carbide [5] ceramics through high-entropy design has sparked significant research dedicated to their synthesis and characterisation. HEB ceramics have been explored in a range of compositions, including $(HfZrTaNbTi)B_2$ [6], $(HfMoZrNbTi)B_2$ [7], $(HfZrTiTaCr)B_2$ [8]. In contrast, various HEC ceramics compositions, such as (HfNbTaTiZr)C [9], (MoNbTaWV)C [10], and (TiZrNbTaW)C [11], have also been studied extensively. The works on the HEB and HEC ceramics have confirmed that the high entropy concept provides excellent opportunities for UHTC ceramics with a broad range of characteristics and applications.

Among the studied compositions, $(HfNbTaTiZr)B_2$ HEB and (HfNbTaTiZr)C HEC have been most extensively studied recently, due to their exceptional properties. $(HfZrTaNbTi)B_2$ HEB, like the other high-entropy diborides, forms an AlB_2-type hexagonal crystal structure [8,12], exhibiting impressive hardness in the range of 18.3–26 GPa (measured at the load of 2 N) [13]. Moreover, the fracture toughness and flexural strength were reported to be 4.35 $MPa.m^{1/2}$ and 388 MPa, respectively [14]. Gild et al. studied the oxidation behaviour of various high-entropy borides and conventional metal mono-borides, which were fabricated and tested in the same conditions [4]. The results showed that $(HfNbTaTiZr)B_2$ HEB exhibited superior oxidation resistance over conventional metal single-diborides. On the other hand, (HfNbTaTiZr)C HEC crystallises into a rock salt FCC crystal structure, and its mechanical properties, such as hardness, fracture toughness, Young's modulus, and flexural strength, were reported to be 32.1 MPa [15], 5.9 $MPa.m^{1/2}$ [16], 479 GPa [17], and 438 MPa [15], respectively. Feng et al. demonstrated

* Corresponding author.
E-mail address: peter.tatarko@savba.sk (P. Tatarko).

https://doi.org/10.1016/j.oceram.2025.100792
Received 8 January 2025; Received in revised form 4 April 2025; Accepted 29 April 2025
Available online 30 April 2025

that (HfNbTaTiZr)C HEC exhibited better strength retention at high temperatures when compared to individual single-carbides [18]. However, owing to intrinsic brittleness and challenges in the fabrication of large sizes and complex shapes of ceramics in general, extending the potential application of these high entropy ceramics is related to the development of reliable, user-friendly, and strong joints [19,20].

Brazing is a simple and convenient technique that is frequently used to join boride and carbide ceramics either to themselves or dissimilar materials [21–24]. The selection of a suitable metallic filler, while considering the application condition, plays a crucial role in the brazing of ceramics. Various kinds of active metallic fillers, such as AgCuTi [25], TiNi [26], AlTi [27], and ZrCuNb [28] have been adopted to braze pressure-less sintered SiC, TiB_2-TiC-SiC composite, CVD-SiC, and reaction-sintered SiC ceramics, respectively. Due to its good wettability, low brazing temperature, and reaction bonding formation, a commercial AgCuTi alloy has been widely utilised in the brazing of ceramics to similar [29,30] or dissimilar (metallic) [31–33] materials.

Field-Assisted Sintering Technique (FAST) has proven advantageous for joining of ceramics via both pressureless and pressure-assisted methods [34,35]. Its rapid heating and cooling rates, precise temperature control, and shorter processing times facilitate tailored microstructures and minimize interfacial reactions, ultimately enhancing the mechanical properties of the resulting brazed joints [36].

The investigation of wetting angle and interfacial behaviour of metal/ceramic systems is a crucial study for the development of an appropriate brazing process for ceramics. The interaction between metals and ceramic surfaces, particularly the wetting behaviour of metals on ceramics, has been extensively investigated. In principle, metal-like ceramics, such as diborides and carbides, should be readily wetted by liquid metals; however, the wetting can be limited by the presence of native oxide layers on the ceramic surfaces [37]. Indeed, pure metals, such as Cu and Ag, exhibited poor wettability on the surface of borides and carbides, and a large scatter of data exists depending on experimental parameters and ceramic conditions [38]. It was reported that the contact angle of molten Cu and Ag on the surface of ZrB_2 was 80° and 130°, respectively [39,40]. Passerone et al. reported the wetting angles of 91° and 115° for the wetting of TiB_2 by molten Cu and Ag, respectively [41]. Frage et al. also reported non-reactive wetting for molten Cu (contact angle ~ 90°) and Ag (contact angle ~ 120°) on TiC substrates [42]. The addition of active metals, such as Ti, into pure metals is an efficient way to improve wettability [43,44]. Zhang et al. demonstrated that adding 50 at.% Ti into Cu reduced the contact angle with ZrB_2 substrates from 80° to < 10° [44]. Muolo et al. reported a contact angle of 25° for the molten AgCuTi alloy on the surface of ZrB_2 [45]. Additionally, AgCuTi on the surface of SiC exhibited good wetting with a contact angle < 15° [46]. In this light, AgCuTi could be considered a promising filler for brazing boride and carbide ceramics.

The aim of the present work was to join (HfNbTaTiZr)B_2 HEB and (HfNbTaTiZr)C HEC ceramics to themselves using AgCuTi as the brazing filler. These two ceramics were selected because they are the most widely studied representatives of the HEB and HEC groups. While both ceramics share the same metallic elements, they differ in their structures and chemical bonding, which may result in distinct wetting and interfacial reaction behaviour. To provide a comprehensive understanding of brazing high entropy UHTCs with a common brazing filler (AgCuTi), both materials were investigated in the present study. First, the wettability and interfacial layer of pure Cu and AgCuTi alloy on the surface of ceramics were investigated using the sessile drop technique. The wetting study of pure Cu was conducted to provide a baseline for understanding the fundamental wetting behaviour of the ceramics without the influence of Ti, the active element in AgCuTi. This helps to quantify the effectiveness of Ti in overcoming the inherent wetting challenges associated with high-entropy ceramics. Subsequently, AgCuTi alloy was used to braze the ceramics using pressure-less Field Assisted Sintering Technique, which helps to minimize interfacial reactions and prevent substrate dissolution due to the shortened processing time and rapid heating. This is the first systematic study on the wetting behaviour and interfacial reactivity of Cu and AgCuTi alloy in contact with high entropy ceramics, followed by successful brazing using AgCuTi filler.

2. Materials and methods

2.1. Materials

The (HfTaZrNbTi)B_2 HEB and (HfTaZrNbTi)C HEC ceramics for wetting and brazing experiments were prepared using FAST process, as described in [47] and [48], respectively. Briefly, the oxide powders (all from ThermoFisher Scientific), such as TiO_2 (~ 325 mesh, anatase, 99.6%), ZrO_2 (~ 325 mesh, 99.7%), HfO_2 (~ 325 mesh, 99%), Nb_2O_5 (~ 325 mesh, 99.9%), Ta_2O_5 (~ 325 mesh, 99.85%) were mixed with the B_4C (d50 = 0.5 μm, Grade HD20, H.C. Starck) and carbon black (~ 325 mesh, Vulcan PF, CS Cabot) powders in the molar fraction of 1/1/1/0.5/0.5/3.125/5.95 to synthesise pure HEB phase via boro/carbothermal reduction. The pressure-less synthesis was performed in a FAST machine (DSP 507, Dr. Fritsch) at 1800 °C for 1 hour in a vacuum. Then, the as-synthesised powder was filled up in a graphite die with an inner diameter of 20 mm, and sintered under argon at 1900 °C for 10 min using the uniaxial pressure of 70 MPa. On the other hand, HEC was prepared using a one-step synthesis/sintering process. The HfC (99.5 %, ~ 325 mesh, Alfa Aesar), ZrC (99.5 %, ~ 325 mesh, Alfa Aesar), TaC (99.5 %, ~ 325 mesh, Alfa Aesar), NbC (99 %, < 10 μm, Alfa Aesar), and TiC (99.5 %, typically ~ 2 μm, Alfa Aesar) powders were mixed in an equimolar ratio. The powder mixture was placed in a graphite die with an inner diameter of 20 mm and sintered by FAST in argon at the temperature of 2050 °C for 7 min using the uniaxial pressure of 70 MPa.

After sintering, the samples were cut to a rectangular shape with the dimensions of 12 × 12 × 3 mm^3, and the surface of the samples (12 × 12 mm^2) was polished up to the final 3 μm diamond suspension. The surface roughness (Sa) of the polished ceramics was measured using a non-contact confocal profilometer (Sensofar S-Neox) over an area of 875 × 659 $μm^2$, resulting in the values of less than 30 nm for all ceramic surfaces used for wetting and brazing experiments.

A commercial pure Cu metal (purity: 99.999%, Koch-Light) and a commercial AgCuTi alloy (Ag: 70.5, Cu: 26.5, Ti: 3.0 wt%, Degussa) in the form of foil with a thickness of 100 μm were used as the raw materials for wetting studies and brazing of high entropy ceramics.

2.2. Wetting studies

The wetting experiments were designed based on the sessile-drop technique. The setup consists of two concentric, horizontal alumina tubes connected to the high vacuum rotary and turbo-molecular pump system [27]. To avoid oxygen contamination and remove any species adsorbed to the alumina chamber, the setup was maintained at a high vacuum (4 × 10^{-4} Pa) at 800 °C for 24 h prior to the wetting experiments. Subsequently, the furnace was heated to the final wetting temperature, and an Ar + 5% H_2 gas mixture was introduced into the reactor at a flow rate of 8.33 × 10^{-7} m^3/s. The system was held at the temperature for 10 min to reach a physicochemical equilibrium. After equilibration, the metal/ceramic couple, surrounded by a zirconium foil getter to further reduce potential oxygen contamination around the drop, was positioned in the high-temperature zone through an external manipulator. An S-type thermocouple under the alumina support constantly monitored the experiment temperature. A high-resolution CCD camera was used to record the isothermal wetting process by capturing images every second. After 5 min, the metal/ceramic couple was removed from the furnace hot zone within 20 s and cooled down to room temperature. The ad hoc designed ASTRA View image analysis software was employed to obtain contact angle (θ) data during each experimental run. The wetting experiment of pure Cu and AgCuTi alloy on high entropy ceramics was performed at 1100 °C and 950 °C, respectively. For adequate melting, the wetting temperature for Cu was set 15 °C above its

melting point. On the other hand, the wetting temperature for AgCuTi alloy was chosen based on thermodynamic calculations [49], which highlighted the role of Ti activity in determining contact angles and the interaction between two liquid phases within the miscibility gap (910–950 °C) during the wetting process.

2.3. Brazing procedure

The brazing assembly was achieved by placing the AgCuTi foil with a thickness of 100 μm between two high entropy ceramic substrates (12 × 12 × 3 mm^3) in a graphite die having a diameter of 20 mm. The samples were joined along the 12 × 12 mm^2 surface with an offset (the deliberate misalignment of their edges, with one sample shifted 3 mm laterally relative to the other), corresponding to the joining area of 9 × 12 mm^2. The brazing was performed at 950 °C for 5 min in an Ar atmosphere using a FAST machine (DSP 507, Dr. Fritsch), where any necessary contact pressure was applied to the graphite die, while no pressure was applied to the brazing assembly. The heating and cooling rates were kept constant at 100 °C/min and 20 °C/min, respectively.

2.4. Characterisation

The phase compositions of the as-sintered HEB and HEC ceramics were characterised using X-ray diffraction (XRD; Panalytical Empyrean, Cu Kα radiation). The microstructure and chemical compositions of the as-sintered materials were investigated using a Scanning Electron Microscope (SEM; AURIGA Compact, Zeiss), while the interfacial layers of the ceramic/metal couples after wetting and brazing were characterised by SEM (Lyra 3 XMU FEG, Tescan) equipped with an Energy Dispersive Spectroscopy (EDS, Ultimmax, Oxford Instruments) detector.

The strength of the brazed samples was evaluated by a single lap offset shear test, using a universal testing machine (SINTEC D/10) at room temperature [50]. A shear load was applied by moving the cross-head at a speed of 0.5 mm/min. The test configuration and the geometry of the fixture are reported in Ref. [51]. The apparent shear strength was obtained by dividing a maximum force by the brazing area (~ 9 × 12 mm^2) and the average value of at least three measurements was reported. The results of the mechanical tests were expressed as mean ± standard deviation.

3. Results and discussion

3.1. Characterisation of HEC and HEB ceramic substrates

Fig. 1 shows the Secondary Electron SEM images (SEM-SE) of the microstructure of the sintered (HfTaZrNbTi)B_2 HEB and (HfTaZrNbTi)C HEC ceramics, along with their XRD patterns. The XRD results confirmed that the sintered (HfTaZrNbTi)B_2 HEB crystallised into a hexagonal phase, while the sintered (HfTaZrNbTi)C HEC exhibited a single-phase solid solution with a rock-salt structure. Additionally, the SEM images of the microstructures of HEB (Fig. 1a) and HEC (Fig. 1b) confirmed that the sintered high entropy ceramics were nearly fully dense. The single-phase final microstructure was confirmed for both the HEB and HEC by XRD, as shown in Fig. 1c. Detailed information regarding the development and characterisation of HEB [47] and HEC [48] ceramics was provided in our previous works.

3.2. Wetting of pure Cu on HEB and HEC ceramics

Figs. 2a and 2b illustrate the wetting behaviour of pure Cu on (HfTaZrNbTi)B_2 HEB and (HfTaZrNbTi)C HEC ceramic substrates, respectively, while Figs. 2c and 2d show the SE-SEM images of the cross-sections of the metal/ceramic couples. This experiment was conducted at 1100 °C, which is 15 °C above the melting point of copper (1085 °C). The laplacian curvature observed in the shape of the droplets confirmed that melting had occurred. It can be observed that pure Cu exhibited poor wettability on both ceramics, reaching final contact angles of 120° and 126° for HEB and HEC, respectively. For the 300 s of liquid-solid contact, the contact angle remained constant. The present results are in good agreement with some previous works reporting the poor wettability of molten pure Cu on boride and carbide ceramics [39,41,42,44]. The weak interfacial bonding and the lack of chemical reactions at the interface mainly cause the poor wetting of molten Cu on boride and carbide ceramics. Pure Cu does not form strong bonds or interfacial compounds with these relatively stable ceramics, which prevents the surface energy reduction needed for good wetting. As a result, strong atomic bonds in carbide and boride ceramics leads to a high contact angle, even at elevated temperatures [39,41,42].

3.3. Wetting of AgCuTi alloy on HEB and HEC ceramics

Fig. 3 presents the time-dependent changes in the contact angle during the wetting of molten AgCuTi alloy on HEB and HEC ceramic surfaces. This also shows the macro images of the ceramic/molten metal couples captured at various time intervals, ranging from 0 s to 300 s. It is clear that in comparison with Cu, AgCuTi showed a good wettability on the surface of both the HEB and the HEC ceramics with the final contact angle of ≤ 17° after 300 s. In both cases, the wetting kinetics suggest that liquid spreading on the substrates was driven by interfacial interactions. In the case of HEB ceramics, the wetting angle rapidly decreased to ~ 50° within the initial 50 s. Subsequently, the molten alloy continued to spread, with the contact angle gradually decreasing to a final value of ≤ 17° over the following 240 s. Similarly, in the case of HEC ceramics, the wetting angle sharply dropped to ~ 60° in about 40 s, followed by a stepwise reduction in the contact angle over time. The final contact angle of 17° was reached after approximately 180 s, which then remained stable until the end of the test. This slightly different evolution of contact angle observed for the two high-entropy ceramic substrates can be attributed to the slightly enhanced reactivity of the molten alloy with the HEC substrate, as will be discussed later. It should be pointed out that somewhat different kinetics did not influence the final contact angle and overall spreading behaviour of the molten alloy on the two ceramic substrates, as clearly shown in Fig. 3.

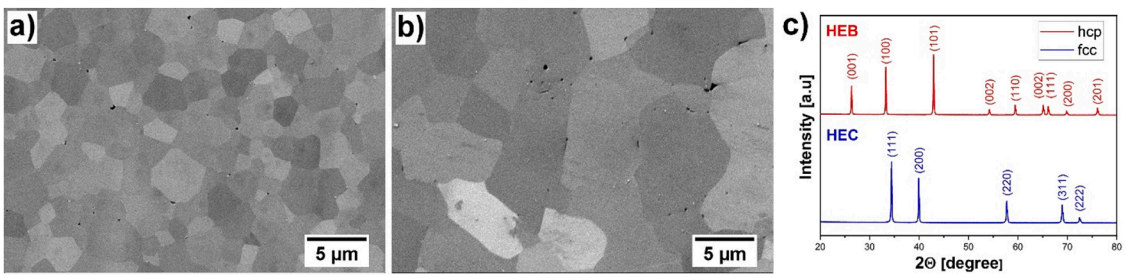

Fig. 1. SEM-SE microstructure of the sintered HEB (a) and HEC (b) used for wetting and brazing experiments. XRD patterns confirmed the formation of a single-phase solid solution in both ceramics (c).

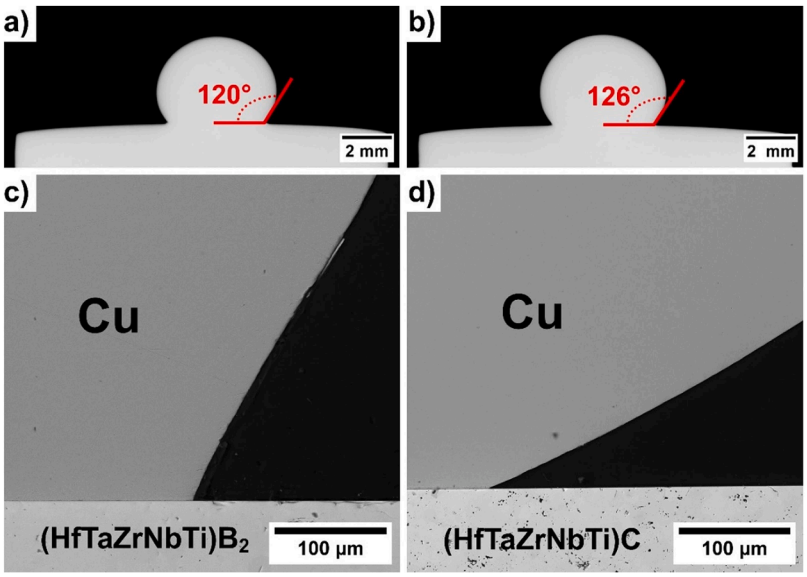

Fig. 2. Macro images of molten Cu on the surface of HEB (a) and HEC (b). SEM-SE image of the interface between the solidified Cu and HEB (c) and HEC (d) surfaces after wetting at 1100 °C for 5 min.

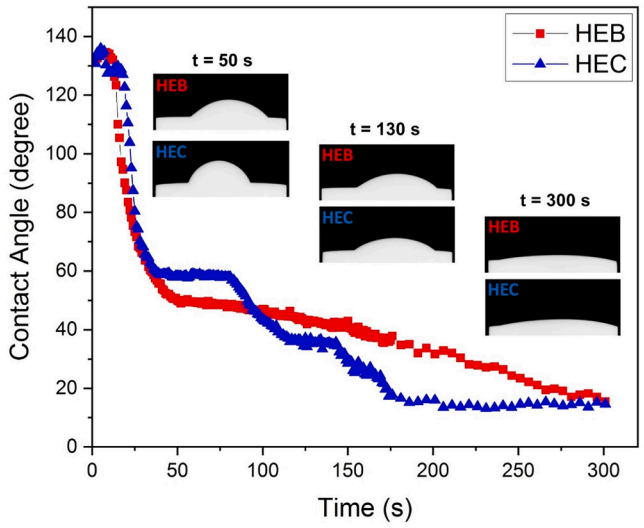

Fig. 3. Contact angle as the function of time during the wetting experiment of molten AgCuTi alloy on the surface of HEB (in red) and HEC (in blue) performed at 950 °C.

3.4. Microstructure, interfacial reactions, and brazing of HEB ceramics

Fig. 4 shows the back-scattered SEM (SEM-BSE) images of the cross-section of the AgCuTi/HEB couple (Fig. 4a) and the detailed interfacial microstructures at different magnifications (Fig. 4b-4d) with the corresponding EDS line analysis after the wetting experiment at 950 °C (Fig. 4e). Table 1 shows the EDS results recorded at different regions of the sample interface (shown as A - D in Fig. 4c and 4d) to identify the individual phases. The AgCuTi alloy solidified with a typical eutectic microstructure, along with the formation of elongated Cu-Ti intermetallic compounds. The bright matrix consisted of Ag-rich phase (A), while three distinct Cu-Ti phases were observed in the interfacial regions. The Cu-rich Cu-Ti phase (B) was formed close to the interface with the ceramics (Cu: 76.1 at.%, Ti: 21.9 at.%; likely Cu_4Ti), and some needle-like Cu-Ti grains (C) with a lower amount of Cu (Cu: 54.3 at.%, Ti: 43.7 at.%; likely Cu_4Ti_3) were embedded in this reaction zone. Besides this, the black particles of different shapes (D) were identified as Ti-rich Cu-Ti phase (likely $CuTi_2$). The formation of the same phases as reported in Table 1 has been previously reported in the literature [52–54]. At the interface with ceramics, a Ti-rich continuous interfacial reaction layer with a thickness of ~ 1 μm was observed (Fig. 4d, dark region), also confirmed by the EDS line analysis (Fig. 4e). This is presumably Ti-B phase, but boron cannot be reliably detected by EDS analysis. Additionally, a Ag-rich layer (bright phase in Fig. 4d) with a thickness of ~ 1.5 μm was observed along the interface above the Ti-B layer, as confirmed by the EDS line analysis (Fig. 4e).

The formation of a Ti-rich reaction layer across the ceramic/metal interface indicates that Ti, as an active element in the brazing alloy, played a significant role in improving the wettability of the AgCuTi on the HEB substrate. This behaviour, leading to the formation of Ti-B reaction layer, was previously reported in the studies focused on single diborides [37,38]. The SEM analysis also revealed the presence of some cracks in the ceramic part, which were caused by the thermal expansion coefficient (CTE) mismatch between HEB (the available CTE value is for $(Ti,Zr,Hf)B_2 \sim 8.7 \times 10^{-6}\ K^{-1}$) [55] and AgCuTi alloy (CTE ~ $18 \times 10^{-6}\ K^{-1}$ [49]). The rapid quenching of the samples (within ~ 50 s) after the wetting experiment could exacerbate the effect of the CTE mismatch, leading to the significant formation of cracks due to the residual stresses.

A low contact angle, combined with a strong interaction between AgCuTi alloy and HEB, indicated that AgCuTi is a promising filler for brazing of HEB ceramics. Fig. 5 shows the backscattered SEM images and the corresponding EDS elemental mapping of HEB ceramics brazed with the AgCuTi interlayer at 950 °C within 5 min. The HEB samples were successfully brazed without any defects either in the filler or at the interfacial layer. Contrary to the significant cracking during the wetting experiments, a crack-free joint was achieved due to a relatively slow cooling rate from the brazing temperature in a FAST machine (20 °C/min).

The presence of active element (Ti) within the AgCuTi alloy led to the partial dissolution of the HEB ceramics. Consequently, Hf and Ta were released and incorporated into the filler, forming a Cu(Hf,Ta) solid solution with a minor concentration of Ti (Fig. 5). Notably, the interaction between Ti and the $(HfTaZrNbTi)B_2$ ceramics at the ceramic interface resulted in the development of a (Ti,B)-rich phase. In contrast, the metallic interface exhibited the formation of a relatively thick layer composed of Ti-Cu intermetallic compounds, which aligns with the aforementioned wetting results. The Ag-rich layer, as observed after wetting, was not detected at the joint interface, indicating that the

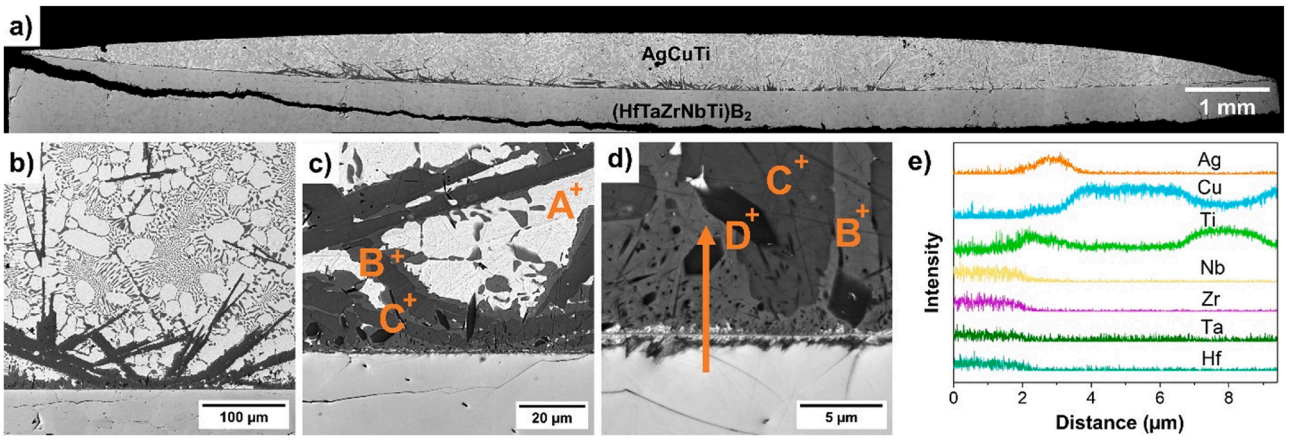

Fig. 4. SEM-BSE images of the cross-section of AgCuTi/HEB couple after wetting at 950 °C for 300 s at different magnifications (a-d). e) EDS line analysis recorded along the arrow in Fig. 4d.

Table 1
EDS analysis (at.%) recorded in the solidified alloy as shown in Fig. 4c and 4d.

EDS points	Ag	Cu	Ti	Possible phases
A	88.1	11.9	–	Ag (s,s)
B	2.0	76.1	21.9	Cu_4Ti
C	2.0	54.3	43.7	Cu_4Ti_3
D	0.8	32.2	67.0	$CuTi_2$

prolonged exposure to elevated temperature during brazing promoted elemental interdiffusion and the evolution of more homogeneous solid solutions.

Thermodynamic calculations confirmed that Hf tends to dissolve in liquid Cu and form stable phases [56,57]. Turchanin et al. measured the standard enthalpies of solutions of Ti, Zr, and Hf in liquid Cu and demonstrated that the Cu-Hf compound is more stable than Cu-Ti or Cu-Zr compounds [58]. The dissolution of Ta below 1084 °C in molten Cu is negligible and does not form any intermetallic compounds [59,60], and its solubility behaviour is affected by the presence of impurities or other refractory metals [61]. The present results indicate that the presence of other elements, such as B, or Hf, significantly affected the solubility of Ta in liquid Cu, resulting in the formation of Cu(Hf,Ta,Ti) solid solution (see Fig. 5).

3.5. Microstructure, interfacial reactions, and brazing of HEC ceramics

Fig. 6 shows the back-scattered SEM images of the cross-sectioned AgCuTi/HEC system (Fig. 6a), and the interfacial microstructures at different magnifications (Fig. 6b-6d) with the corresponding EDS line analysis after the wetting experiment at 950 °C (Fig. 6e). Moreover, Table 2 shows the results of EDS point analysis of the different phases, as shown in Fig. 6c and 6d. The solidified alloy exhibited the characteristic eutectic microstructure of AgCuTi, consisting of a Ag-rich matrix (labelled "A" in Fig. 6c) and Cu-Ti intermetallic phases. Near the interface, three distinct Cu-Ti intermetallic phases were observed. A Ti-rich Cu-Ti intermetallic phase (labelled "D") formed an almost continuous layer directly at the interface. Adjacent to this, a core-shell structure of Cu-Ti intermetallic phases with varying Ti and Cu content in the core ("C") and the shell ("B") was observed. Consistent with the HEB/AgCuTi system, the formation of Cu(Hf,Ta,Ti) solid solution within the solidified alloy (indicated as C) was confirmed by EDS line scan (Fig. 6e) and point analysis (Table 2). EDS analysis (Fig. 6d, Table 2) further confirmed that Ti acted as active element, reacting significantly with the HEC substrate to form a continuous Ti-rich reaction layer (labelled "E") containing a significant amount of Ta and Nb. This suggests that a complex carbide phase was formed. Notably, this reaction layer was thicker (2.5 – 3 μm) compared to the HEB/AgCuTi system, indicating a higher reactivity of the alloy with the HEC surface. The resulting "rougher" interface likely contributed to the step-like evolution of contact angles observed during wetting experiments on the HEC substrates (Fig. 3). At the same time, a

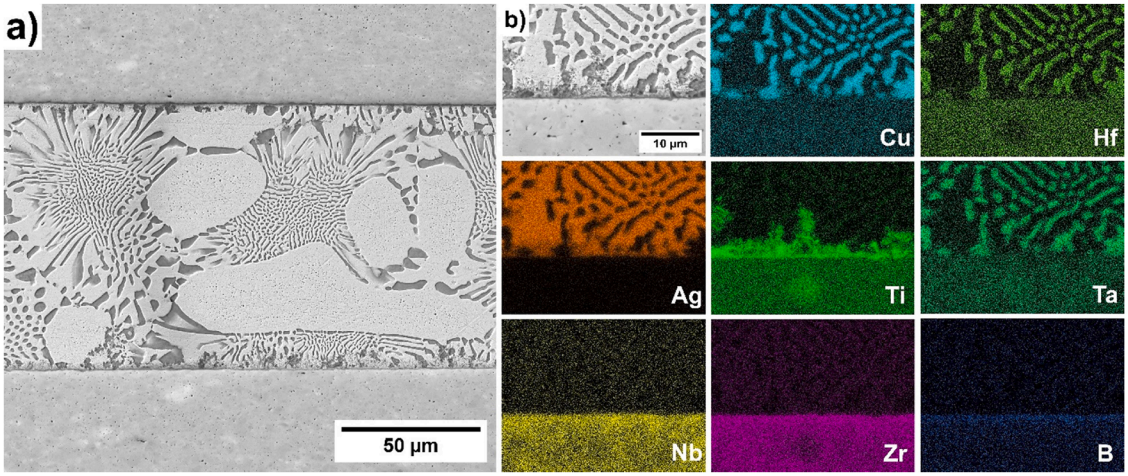

Fig. 5. SEM-BSE image of the cross-section of HEB/AgCuTi/HEB joint (a) and the corresponding EDS mapping (b).

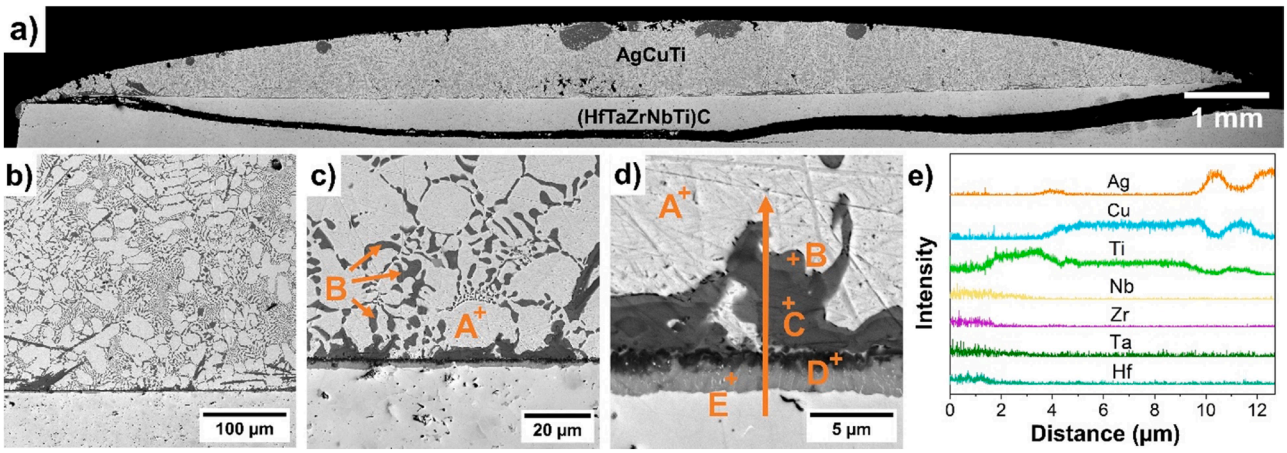

Fig. 6. SEM-BSE images of the cross-section of AgCuTi/HEC couple after wetting at 950 °C for 300 s at different magnifications (a-d). e) EDS line analysis recorded along the arrow shown in Fig. 4d.

Table 2
EDS analysis (at.%) recorded at the points reported in Fig. 6c and 6d (carbon was excluded from the analysis).

EDS points	Ag	Cu	Ti	Hf	Ta	Zr	Nb	Possible phases
A	78.5	12.2	2.2	1.7	2.8	1.4	1.2	Ag (s,s)
B	17.3	55.0	18.3	2.3	4.4	1.4	1.3	–
C	2.8	49.5	40.2	1.9	3.6	0.9	1.2	–
D	9.1	18.3	60.6	2.5	3.8	2.7	3.1	–
E	1.6	3.8	63.7	4.5	11.0	3.3	12.2	$(Ti,Nb,Ta)C_x$

significantly lower amount and a smaller size of Cu-Ti intermetallic phases was formed in the HEC/AgCuTi system.

Fig. 7 shows the microstructure of the HEC samples joined with the AgCuTi filler at 950 °C, along with the corresponding EDS elemental mapping. Similar to the HEB/AgCuTi system, a Ti-rich layer was formed at the metal/ceramics interface. It has already been reported that when AgCuTi alloy is in contact with carbide ceramics, active Ti within the alloy reacts with the ceramic substrate to form carbide phases [30]. Moreover, analogous to the wetting experiment, a Ti reaction layer, also containing Nb and Ta, was detected at the ceramic part of the interface. This reaction layer (containing $(Ti,Nb,Ta)C_x$ phases) exhibited a greater thickness (2.5 – 3.0 μm) in the HEC/AgCuTi system when compared to the TiB_x reaction layer found in the HEB/AgCuTi system (1.0 – 1.5 μm). This finding aligns with the wetting results presented in Fig. 3. As previously discussed for the HEB/AgCuTi system, Hf and Ta from the ceramic substrate dissolved into molten Cu to form a Cu(Hf,Ta) solid solution, which also contained a minor amount of Ti (Fig. 7). In agreement with the wetting results, the HEC/AgCuTi/HEC joints exhibited a significantly smaller amount of Ti-Cu intermetallic phases at the metallic part of the interface (Fig. 7) when compared to the HEB/AgCuTi/HEB joints (Fig. 5).

3.6. *Mechanism of brazing*

The brazing mechanism of HEB and HEC ceramics with AgCuTi alloy was determined through chemical composition and microstructural analysis, revealing a three-stage process: i. Melting of the AgCuTi alloy and initial contact, ii. Atomic diffusion and interfacial reactions, and iii. Precipitation of new phases and joint formation. While both ceramics exhibited similar initial behaviours with the molten AgCuTi alloy, their distinct chemical compositions and bonding led to differences in phase formation and reaction layer thickness.

i. Melting of AgCuTi alloy and initial contact: Upon heating, the AgCuTi alloy melts and wets the ceramic substrates. Titanium in the alloy plays a crucial role in enhancing wettability by its reaction with the ceramic surfaces, facilitating initial contact. This observation is consistent with other ceramic brazing systems, such as SiC [30], Si_3N_4 [43] and ZrB_2 [44], where Ti addition improved wettability and initial contact.

ii. Atomic diffusion and interfacial reactions: As brazing progresses, Ti atoms diffuse from the AgCuTi filler towards the ceramic interfaces, initially reacting at grain boundaries. In both HEB and HEC systems, Hafnium and Tantalum from the ceramics dissolve into

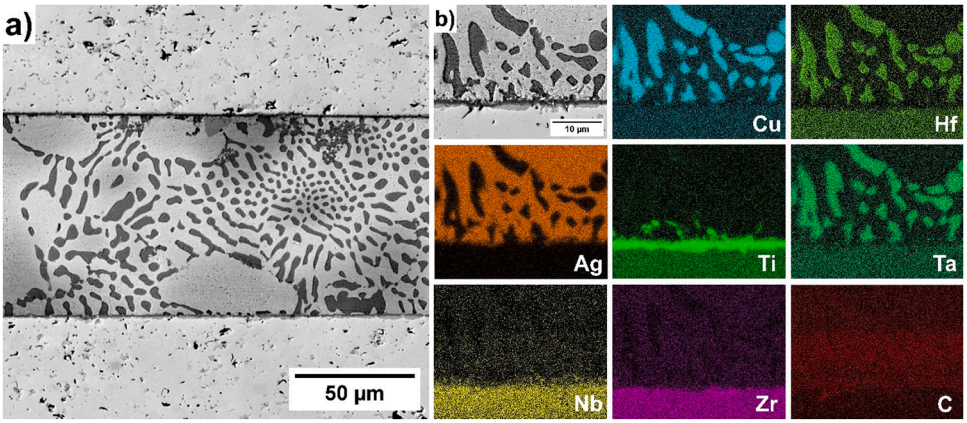

Fig. 7. SEM-BSE images of the cross-section of HEC/AgCuTi/HEC joint (a) and the corresponding EDS mapping (b).

the molten Cu, forming Cu(Hf,Ta) solid solutions [56–58]. However, the strong metal-boron covalent bonds and high thermodynamic stability of HEB limit Ti interaction and boride dissolution, resulting in slower interfacial reaction kinetics and a thinner reaction layer compared to carbide-based ceramics [45,62]. Despite this limitation, Ti reacts slightly with available boron at the HEB interface, forming TiB_x phases, similar to observations in $CuTi/TiB_2$ [63] and $AlMgB_{14}$-TiB_2/AgCuTi [64] systems. Conversely, the high reactivity of Ti with carbon in HEC promotes significant interfacial reactions, increasing material dissolution and enriching the molten alloy with transition metals. This enhanced reactivity leads to the enrichment of transition metal elements from the ceramic in the molten alloy, facilitating their incorporation into the interfacial Cu-Ti reaction zone. As a result, a higher amount of elemental interdiffusion is observed, influencing the interfacial chemistry and microstructural evolution. This behaviour aligns with studies on brazing of SiC [29], ZrC-SiC [33] ceramics, where Ti reacts with carbon to form carbide phases.

iii. Precipitation of new phases and joint formation: As the alloy and interface stabilize during cooling, the elements reprecipitate, forming complex intermetallic phases at both interfaces: borides at the HEB/AgCuTi interface, and carbides at the HEC/AgCuTi interface. Solidification of these in-situ formed metallic, intermetallic and ceramic phases significantly affect mechanical bonding by reducing interfacial energy [37,39,44]. In the HEB/AgCuTi system, a thin (~1 μm) Ti-B reaction layer precipitates, with minimal Ag-rich layer formation, indicating the dominance of the Ti-rich reaction layer in bonding. In contrast, the HEC/AgCuTi system exhibits a thicker (~2.5 – 3 μm) reaction layer composed of complex (Ti,Nb,Ta)Cx carbide phases. The presence of Ta and Nb in HEC contributes to the thickness and complexity of the reaction layer, enhancing interfacial bonding. It should be noted that Nb and Ta tend to form carbide reaction layer at the interface.

In summary, while both HEB/AgCuTi and HEC/AgCuTi brazing systems share common behaviours, such as the formation of Ti-rich reaction layer and the dissolution of Hf and Ta into the molten Cu to form stable Cu(Hf,Ta) solid solutions, key differences arise due to the distinct chemical compositions and bonding of the individual ceramics. HEB forms thinner (~1 μm) TiB_x phases, whereas HEC forms a thicker (~2.5 – 3 μm) interfacial layer with more complex (Ti,Nb,Ta)C_x phases. These differences in reaction layer thickness and composition significantly influence the mechanical properties of the brazed joints.

3.7. Shear strength of the brazed HEB and HEC ceramics

Fig. 8 shows the apparent shear strength of HEB and HEC ceramics brazed with the AgCuTi alloy at 950 °C. Due to the crack-free, homogenous interlayer, a relatively high apparent shear strength of 116 ± 38 MPa and 176 ± 39 MPa was measured for the HEB/AgCuTi/HEB and HEC/AgCuTi/HEC joints, respectively. It should be pointed out that in all cases, the failure of the joints occurred in the base materials and not in the joining interlayer, or along the interface. Since the base materials crashed and fragmented into many small pieces, a higher number of specimens or the specimens with a reduced joining area would be needed to provide more reliable shear strength of the joints, followed by the fractography. However, the present results clearly revealed that the final shear strength of the joints was pre-determined by the intrinsic strength of the base materials, i.e. (HfTaZrNbTi)B_2 and (HfTaZrNbTi)C. Although a direct comparison between the two high-entropy ceramic substrates is limited by the different intrinsic properties of both materials, the shear strength of the HEC joints was still higher when compared to the HEB joints.

Various strength values for the ceramics brazed with AgCuTi alloy have been reported. Song et al. brazed the SiC samples using AgCuTi filler reinforced with graphene nanoplatelets, achieving a shear strength of 38 MPa [30]. Zhou et al. reported a shear strength of 70 MPa for the SiC joints with AgCuTi alloy prepared using flash joining technique [29]. Yang et al. reported a shear strength of 146 MPa for the ZrB_2-SiC joints with TiB-reinforced AgCuTi alloy [65]. These reported values confirmed that the strength of the ceramic brazed with AgCuTi is strongly related to the thickness, composition, and microstructure of the interlayer, as well as the intrinsic properties of the base materials.

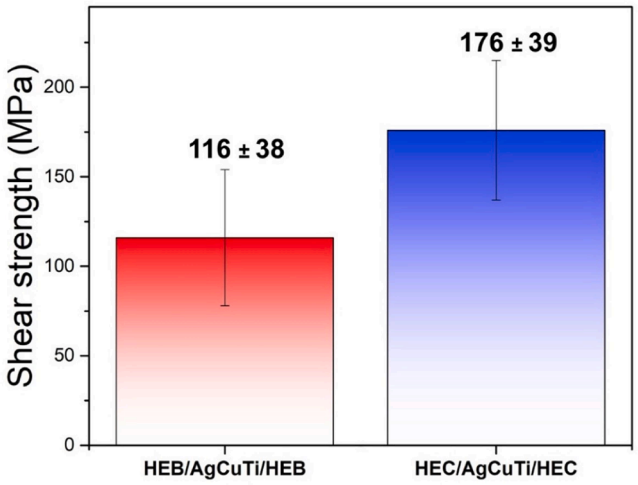

Fig. 8. Apparent shear strength of HEB and HEC ceramics brazed with AgCuTi at 950 °C.

Therefore, the relatively high shear strength achieved in this work can be attributed to the well-densified, single-phase HEB and HEC ceramic substrates, along with the formation of crack-free reaction layer. Specifically, a TiB_x-rich layer formed in the HEB/AgCuTi/HEB joint, while a (Ti,Nb,Ta)C_x-rich layer developed in the HEC/AgCuTi/HEC joint, both contributing to the enhanced mechanical performance. In addition, the Cu-Ti intermetallic compounds are well known as brittle phases and their presence leads to the deterioration of the strength. In the present work, the formation of these brittle intermetallic compounds was partially inhibited, particularly in the case of HEC joints, which could also significantly contribute to the higher strength of the joints.

4. Conclusion

The wettability and interfacial interaction of molten Cu and AgCuTi alloy on the surface of (HfTaZrNbTi)B_2 HEB and (HfTaZrNbTi)C HEC ceramics were investigated for the first time, allowing to draw the following conclusions:

1) Pure Cu exhibited a poor, non-reactive wetting on both the HEB (contact angle of 120°) and HEC (contact angle of 126°) substrates, indicating poor interfacial adhesion. In contrast, the AgCuTi alloy exhibited significant reactive wetting on both substrates (contact angle ≤ 17°), making it a suitable filler for brazing of HEB and HEC ceramics.
2) The high-temperature interaction between the molten AgCuTi alloy and the HEC ceramic substrate resulted in the formation of a thicker (Ti,Nb,Ta)C_x reaction layer (2.5 – 3.0 μm) when compared to the thinner TiB_x reaction layer (1.0 – 1.5 μm) observed at the interface with the HEB substrate. This difference highlights the distinct interfacial reactivity of the AgCuTi alloy with the two ceramic types.
3) The apparent shear strength of HEC and HEB joints was 176 ± 39 MPa and 116 ± 38 MPa, respectively. In all tested joints, failure consistently occurred within the base ceramic materials, which showed extensive fragmentation. This failure mode suggests that the measured shear strength of both joints was limited by the inherent

mechanical strength of the HEB and HEC ceramics themselves, rather than the integrity of the brazed interface.

4) This study provides a fundamental understanding for the development of effective joining methodologies for these novel high-entropy boride and carbide ceramics. The demonstrated ability of brazing with AgCuTi alloy opens avenues for their integration into advanced technological applications requiring robust performance in extreme service environments.

CRediT authorship contribution statement

Naser Hosseini: Writing – original draft, Visualization, Investigation, Data curation, Conceptualization. **Fabrizio Valenza:** Writing – review & editing, Visualization, Validation, Data curation, Conceptualization. **Zdeněk Chlup:** Validation, Methodology, Data curation. **Sofia Gambaro:** Writing – review & editing, Visualization, Investigation. **Carla Malinverni:** Investigation. **Valentina Casalegno:** Methodology, Investigation, Data curation. **Alexandra Kovalčíková:** Investigation. **Monika Tatarková:** Investigation, Funding acquisition, Data curation. **Ivo Dlouhý:** Validation, Funding acquisition, Formal analysis. **Peter Tatarko:** Writing – review & editing, Visualization, Validation, Supervision, Funding acquisition, Conceptualization.

Declaration of competing interest

The authors declare that they have no known competing financial interests or personal relationships that could have appeared to influence the work reported in this paper.

Acknowledgment

This work was supported by the Slovak research and development agency under the Contract no. SK-CZ-RD-21–0089. The support of LUASK22219 and CNR-SAS-2024–03 projects is also acknowledged. The authors are grateful to the JECS Trust for funding [the visit of Naser Hosseini to ICMATE-CNR in Genoa.] (Contract No. 2022334).

References

[1] T.C. Dube, J. Zhang, Underpinning the relationship between synthesis and properties of high entropy ceramics: a comprehensive review on borides, carbides and oxides, J Eur Ceram Soc 44 (2024) 1335–1350, https://doi.org/10.1016/j.jeurceramsoc.2023.10.023.

[2] Z. Wang, Z.-T. Li, S.-J. Zhao, Z.-G. Wu, High-entropy carbide ceramics: a perspective review, Tungsten 3 (2021) 131–142, https://doi.org/10.1007/s42864-021-00085-7.

[3] S. Akrami, P. Edalati, M. Fuji, K. Edalati, High-entropy ceramics: review of principles, production and applications, Materials Science and Engineering: R: Reports 146 (2021) 100644, https://doi.org/10.1016/j.mser.2021.100644.

[4] J. Gild, Y. Zhang, T. Harrington, S. Jiang, T. Hu, M.C. Quinn, W.M. Mellor, N. Zhou, K. Vecchio, J. Luo, High-Entropy Metal Diborides: a New Class of High-Entropy Materials and a New Type of Ultrahigh Temperature Ceramics, Sci Rep 6 (2016) 37946, https://doi.org/10.1038/srep37946.

[5] E. Castle, T. Csanádi, S. Grasso, J. Dusza, M. Reece, Processing and Properties of High-Entropy Ultra-High Temperature Carbides, Sci Rep 8 (2018) 8609, https://doi.org/10.1038/s41598-018-26827-1.

[6] Y. Zhang, Z.-B. Jiang, S.-K. Sun, W.-M. Guo, Q.-S. Chen, J.-X. Qiu, K. Plucknett, H.-T. Lin, Microstructure and mechanical properties of high-entropy borides derived from boro/carbothermal reduction, J Eur Ceram Soc 39 (2019) 3920–3924, https://doi.org/10.1016/j.jeurceramsoc.2019.05.017.

[7] G. Tallarita, R. Licheri, S. Garroni, S. Barbarossa, R. Orrù, G. Cao, High-entropy transition metal diborides by reactive and non-reactive spark plasma sintering: a comparative investigation, J Eur Ceram Soc 40 (2020) 942–952, https://doi.org/10.1016/j.jeurceramsoc.2019.10.031.

[8] J. Gild, A. Wright, K. Quiambao-Tomko, M. Qin, J.A. Tomko, M. Shafkat bin Hoque, J.L. Braun, B. Bloomfield, D. Martinez, T. Harrington, K. Vecchio, P. E. Hopkins, J. Luo, Thermal conductivity and hardness of three single-phase high-entropy metal diborides fabricated by borocarbothermal reduction and spark plasma sintering, Ceram Int 46 (2020) 6906–6913, https://doi.org/10.1016/j.ceramint.2019.11.186.

[9] B. Ye, T. Wen, K. Huang, C. Wang, Y. Chu, First-principles study, fabrication, and characterization of (Hf $_{0.2}$ Zr $_{0.2}$ Ta $_{0.2}$ Nb $_{0.2}$ Ti $_{0.2}$)C high-entropy ceramic, Journal of the American Ceramic Society 102 (2019) 4344–4352, https://doi.org/10.1111/jace.16295.

[10] D. Medved', M. Ivor, A. Kovalčíková, E. Múdra, T. Csanádi, R. Sedlák, H. Ünsal, P. Tatarko, M. Tatarková, P. Šajgalík, J. Dusza, Wear behavior of (Mo–Nb–Ta–V–W)C high-entropy carbide, Int J Appl Ceram Technol 20 (2023) 224–235, https://doi.org/10.1111/ijac.14111.

[11] X.-F. Wei, J.-X. Liu, F. Li, Y. Qin, Y.-C. Liang, G.-J. Zhang, High entropy carbide ceramics from different starting materials, J Eur Ceram Soc 39 (2019) 2989–2994, https://doi.org/10.1016/j.jeurceramsoc.2019.04.006.

[12] H. Chen, H. Xiang, F.-Z. Dai, J. Liu, Y. Zhou, Porous high entropy (Zr0.2Hf0.2Ti0.2Nb0.2Ta0.2)B2: a novel strategy towards making ultrahigh temperature ceramics thermal insulating, J Mater Sci Technol 35 (2019) 2404–2408, https://doi.org/10.1016/j.jmst.2019.05.059.

[13] L. Feng, W.G. Fahrenholtz, G.E. Hilmas, Processing of dense high-entropy boride ceramics, J Eur Ceram Soc 40 (2020) 3815–3823, https://doi.org/10.1016/j.jeurceramsoc.2020.03.065.

[14] L. Qiao, Y. Liu, Y. Gao, J. Bi, Y. Li, C. Liu, J. Gao, W. Wang, Z. Qian, First-principles prediction, fabrication and characterization of (Hf0.2Nb0.2Ta0.2Ti0.2Zr0.2)B2 high-entropy borides, Ceram Int 48 (2022) 17234–17245, https://doi.org/10.1016/j.ceramint.2022.02.281.

[15] P. Istomin, E. Istomina, A. Nadutkin, V. Grass, A. Lysenkov, A. Kudryavtsev, Preparation of (Ti,Zr,Hf,Nb,Ta)C high-entropy carbide ceramics through carbosilicothermic reduction of oxides, J Eur Ceram Soc 41 (2021) 6934–6942, https://doi.org/10.1016/j.jeurceramsoc.2021.07.012.

[16] F. Wang, X. Zhang, X. Yan, Y. Lu, M. Nastasi, Y. Chen, B. Cui, The effect of submicron grain size on thermal stability and mechanical properties of high-entropy carbide ceramics, Journal of the American Ceramic Society 103 (2020) 4463–4472, https://doi.org/10.1111/jace.17103.

[17] X. Yan, L. Constantin, Y. Lu, J. Silvain, M. Nastasi, B. Cui, (Hf $_{0.2}$ Zr $_{0.2}$ Ta $_{0.2}$ Nb $_{0.2}$ Ti $_{0.2}$)C high-entropy ceramics with low thermal conductivity, Journal of the American Ceramic Society 101 (2018) 4486–4491, https://doi.org/10.1111/jace.15779.

[18] L. Feng, W. Chen, W.G. Fahrenholtz, G.E. Hilmas, Strength of single-phase high-entropy carbide ceramics up to 2300 °C, Journal of the American Ceramic Society 104 (2021) 419–427, https://doi.org/10.1111/jace.17443.

[19] M. Ferraris, M. Salvo, V. Casalegno, S. Han, Y. Katoh, H.C. Jung, T. Hinoki, A. Kohyama, Joining of SiC-based materials for nuclear energy applications, Journal of Nuclear Materials 417 (2011) 379–382, https://doi.org/10.1016/j.jnucmat.2010.12.160.

[20] G. Liu, X. Zhang, J. Yang, G. Qiao, Recent advances in joining of SiC-based materials (monolithic SiC and SiCf/SiC composites): joining processes, joint strength, and interfacial behavior, Journal of Advanced Ceramics 8 (2019) 19–38, https://doi.org/10.1007/s40145-018-0297-x.

[21] W. Yang, L. Xing, T. Lin, P. He, J. Lin, X. Ma, Microstructural evolution and growth/degradation behavior of in situ TiB whiskers in ZrB2-SiC joints using Ti/Ni/Ti filler, J Alloys Compd 744 (2018) 124–131, https://doi.org/10.1016/j.jallcom.2018.02.054.

[22] Y. Song, D. Liu, S. Hu, X. Song, Y. Lei, J. Cao, Brazing of metallized SiC ceramic to GH99 superalloy using graphene nanoplatelets reinforced AgCuTi composite filler, Ceram Int 45 (2019) 8962–8970, https://doi.org/10.1016/j.ceramint.2019.01.227.

[23] Y. Wang, K. Zhang, D. Yin, Composite brazing of high thermal mismatched Cf/SiC and 304 stainless steel with foil (Cu) + Ti5Si3 alloy as filler, Mater Lett 351 (2023) 135015, https://doi.org/10.1016/j.matlet.2023.135015.

[24] J. Wu, J. Yan, H. Peng, D. Bai, H. Shi, Z. Liu, R. Zhang, M. Li, Y. Wen, N. Li, Reaction mechanism and mechanical properties of SiC joint brazed by in-situ formation of Ti3SiC2, J Eur Ceram Soc 44 (2024) 3777–3783, https://doi.org/10.1016/j.jeurceramsoc.2023.12.097.

[25] X. Dai, J. Cao, Y. Tian, Z. Chen, X. Song, J. Feng, Effect of holding time on microstructure and mechanical properties of SiC/SiC joints brazed by Ag-Cu-Ti + B4C composite filler, Mater Charact 118 (2016) 294–301, https://doi.org/10.1016/j.matchar.2016.06.008.

[26] X.Q. Cai, D.P. Wang, Y. Wang, Z.W. Yang, Microstructural evolution and mechanical properties of TiB2-TiC-SiC ceramics joint brazed using Ti-Ni composite foils, J Eur Ceram Soc 40 (2020) 3380–3390, https://doi.org/10.1016/j.jeurceramsoc.2020.03.053.

[27] F. Valenza, S. Gambaro, M.L. Muolo, M. Salvo, V. Casalegno, Wetting of SiC by Al-Ti alloys and joining by in-situ formation of interfacial Ti3Si(Al)C2, J Eur Ceram Soc 38 (2018) 3727–3734, https://doi.org/10.1016/j.jeurceramsoc.2018.04.025.

[28] Z. Zhang, Y. Cai, Y. Liu, K. Feng, Study on Brazing of SiC Ceramics with Zr-Cu-Nb Filler Metal, J Mater Eng Perform (2023), https://doi.org/10.1007/s11665-023-08501-4.

[29] L. Zhou, C. Li, X. Si, C. Zhang, J. Qi, J. Cao, Flash brazing of SiC using Ag-Cu-Ti alloy at ultra-low temperature in air via electric field assistance, J Eur Ceram Soc 43 (2023) 7708–7713, https://doi.org/10.1016/j.jeurceramsoc.2023.08.002.

[30] Y. Song, D. Liu, S. Hu, X. Song, J. Cao, Graphene nanoplatelets reinforced AgCuTi composite filler for brazing SiC ceramic, J Eur Ceram Soc 39 (2019) 696–704, https://doi.org/10.1016/j.jeurceramsoc.2018.11.046.

[31] S. Gambaro, F. Valenza, A. Passerone, G. Cacciamani, M.L. Muolo, Brazing transparent YAG to Ti6Al4V: reactivity and characterization, J Eur Ceram Soc 36 (2016) 4185–4196, https://doi.org/10.1016/j.jeurceramsoc.2016.05.022.

[32] G. Wang, Y. Cai, Q. Xu, C. Zhou, C. Tan, W. Cao, Microstructural and mechanical properties of inconel 600/ZrB2-SiC joints brazed with AgCu/Cu-foam/AgCu/Ti multi-layered composite filler, Journal of Materials Research and Technology 9 (2020) 3430–3437, https://doi.org/10.1016/j.jmrt.2020.01.080.

[33] J.M. Shi, J.C. Feng, X.Y. Tian, H. Liu, L.X. Zhang, Interfacial microstructure and mechanical property of ZrC-SiC ceramic and Ti6Al4V joint brazed with AgCuTi

alloy, J Eur Ceram Soc 37 (2017) 2769–2778, https://doi.org/10.1016/j.jeurceramsoc.2017.02.056.
[34] S. Grasso, P. Tatarko, S. Rizzo, H. Porwal, C. Hu, Y. Katoh, M. Salvo, M.J. Reece, M. Ferraris, Joining of β-SiC by spark plasma sintering, J Eur Ceram Soc 34 (2014) 1681–1686, https://doi.org/10.1016/j.jeurceramsoc.2013.12.023.
[35] X. Wang, T.G. Saunders, M. Salvo, Y. Wang, X. Xiao, L. Fu, M.J. Reece, Joining graphite with ZrHfNbTa and TiZrHfTa high entropy alloy interlayers by spark plasma sintering, J Mater Process Technol 320 (2023) 118102, https://doi.org/10.1016/j.jmatprotec.2023.118102.
[36] S. Rizzo, S. Grasso, M. Salvo, V. Casalegno, M.J. Reece, M. Ferraris, Joining of C/SiC composites by spark plasma sintering technique, J Eur Ceram Soc 34 (2014) 903–913, https://doi.org/10.1016/j.jeurceramsoc.2013.10.028.
[37] A. Passerone, F. Valenza, M.L. Muolo, A review of transition metals diborides: from wettability studies to joining, J Mater Sci 47 (2012) 8275–8289, https://doi.org/10.1007/s10853-012-6621-x.
[38] S. Bajpai, S. Dubey, T. Venkateswaran, S.S. Singh, K. Balani, An insight to wetting and joining of HfB2 and ZrB2 based ultra high temperature ceramics: a review, Chemical Engineering Journal 495 (2024) 153387, https://doi.org/10.1016/j.cej.2024.153387.
[39] A. Passerone, M.L. Muolo, R. Novakovic, D. Passerone, Liquid metal/ceramic interactions in the (Cu, Ag, Au)/ZrB2 systems, J Eur Ceram Soc 27 (2007) 3277–3285, https://doi.org/10.1016/j.jeurceramsoc.2006.12.008.
[40] F. Valenza, C. Artini, A. Passerone, M.L. Muolo, ZrB2–SiC/Ti6Al4V joints: wettability studies using Ag- and Cu-based braze alloys, J Mater Sci 47 (2012) 8439–8449, https://doi.org/10.1007/s10853-012-6790-7.
[41] A. Passerone, M.L. Muolo, D. Passerone, Wetting of Group IV diborides by liquid metals, J Mater Sci 41 (2006) 5088–5098, https://doi.org/10.1007/s10853-006-0442-8.
[42] N. Frage, N. Froumin, M.P. Dariel, Wetting of TiC by non-reactive liquid metals, Acta Mater 50 (2002) 237–245, https://doi.org/10.1016/S1359-6454(01)00349-4.
[43] R. Klein, M. Desmaison-Brut, P. Ginet, A. Bellosi, J. Desmaison, Wettability of silicon nitride ceramic composites by silver, copper and silver copper titanium alloys, J Eur Ceram Soc 25 (2005) 1757–1763, https://doi.org/10.1016/j.jeurceramsoc.2004.12.005.
[44] X. Zhang, P. Xu, X. Wu, X. Gui, G. Liu, M. Zhang, H. Meng, G. Qiao, Insight into the wetting and interfacial behavior of Cu-Ti/ZrB2 system: a combined experimental and DFT calculation, J Eur Ceram Soc 41 (2021) 6213–6222, https://doi.org/10.1016/j.jeurceramsoc.2021.06.002.
[45] M.L. Muolo, E. Ferrera, A. Passerone, Wetting and spreading of liquid metals on ZrB2-based ceramics, J Mater Sci 40 (2005) 2295–2300, https://doi.org/10.1007/s10853-005-1948-1.
[46] W. Tillmann, J. Pfeiffer, N. Sievers, K. Boettcher, Analyses of the spreading kinetics of AgCuTi melts on silicon carbide below 900 °C, using a large-chamber SEM, Colloids Surf A Physicochem Eng Asp 468 (2015) 167–173, https://doi.org/10.1016/j.colsurfa.2014.12.039.
[47] V. Kombamuthu, H. Ünsal, Z. Chlup, M. Tatarková, A. Kovalčíková, I. Zhukova, N. Hosseini, M. Hičák, I. Dlouhý, P. Tatarko, Effect of SiC on densification, microstructure and mechanical properties of high entropy diboride (Ti0.2Zr0.2Hf0.2Nb0.2Ta0.2)B2, J Eur Ceram Soc 44 (2024) 5358–5369, https://doi.org/10.1016/j.jeurceramsoc.2023.12.072.
[48] J. Dusza, T. Csanádi, D. Medveď, R. Sedlák, M. Vojtko, M. Ivor, H. Ünsal, P. Tatarko, M. Tatarková, P. Šajgalík, Nanoindentation and tribology of a (Hf-Ta-Zr-Nb-Ti)C high-entropy carbide, J Eur Ceram Soc 41 (2021) 5417–5426, https://doi.org/10.1016/j.jeurceramsoc.2021.05.002.
[49] S. Gambaro, M.L. Muolo, F. Valenza, G. Cacciamani, L. Esposito, A. Passerone, Wettability of transparent YAG (Y3Al5O12) by molten Ag–Cu–Ti alloys, J Eur Ceram Soc 35 (2015) 2895–2906, https://doi.org/10.1016/j.jeurceramsoc.2015.03.036.
[50] C. Malinverni, M. Salvo, A. De Zanet, F. D'Isanto, F. Smeacetto, P. Bertrand, G. Puchas, S. Schafföner, V. Casalegno, Glass-ceramics for joining oxide-based ceramic matrix composites (Al2O3/Al2O3-ZrO2) operating under direct flame exposure, J Eur Ceram Soc 43 (2023) 3621–3629, https://doi.org/10.1016/j.jeurceramsoc.2023.02.019.
[51] M. Suess, C. Wilhelmi, M. Salvo, V. Casalegno, P. Tatarko, M. Funke, Effect of pulsed laser irradiation on the SiC surface, Int J Appl Ceram Technol 14 (2017) 313–322, https://doi.org/10.1111/ijac.12655.
[52] J.M. Shi, J.C. Feng, X.Y. Tian, H. Liu, L.X. Zhang, Interfacial microstructure and mechanical property of ZrC-SiC ceramic and Ti6Al4V joint brazed with AgCuTi alloy, J Eur Ceram Soc 37 (2017) 2769–2778, https://doi.org/10.1016/j.jeurceramsoc.2017.02.056.
[53] Y. Fan, J. Fan, C. Wang, Formation of typical Cu–Ti intermetallic phases via a liquid-solid reaction approach, Intermetallics (Barking) 113 (2019) 106577, https://doi.org/10.1016/j.intermet.2019.106577.
[54] M.A. Turchanin, P.G. Agraval, A.R. Abdulov, Thermodynamic assessment of the Cu-Ti-Zr system. I. Cu-Ti system, Powder Metallurgy and Metal Ceramics 47 (2008) 344–360, https://doi.org/10.1007/s11106-008-9026-2.
[55] S. Ye, J. Zhu, P. Li, M. Li, N. Yan, H. Wang, Study on microstructure, mechanical properties and thermal performance of single-phase (Ti,Zr,Hf)B2 solid solution,, Mater Today Commun 34 (2023) 105228, https://doi.org/10.1016/j.mtcomm.2022.105228.
[56] M.A. Turchanin, P.G. Agraval, Thermodynamic assessment of the copper-hafnium system, Powder Metallurgy and Metal Ceramics 47 (2008) 223–233, https://doi.org/10.1007/s11106-008-9008-4.
[57] V.V. Berezutski, M.I. Ivanov, Thermodynamics of binary liquid Cu–Hf alloys, J Alloys Compd 306 (2000) L1–L2, https://doi.org/10.1016/S0925-8388(00)00690-3.
[58] M.A. Turchanin, I.V. Nikolaenko, Enthalpies of solution of titanium, zirconium, and hafnium in liquid copper, J Alloys Compd 236 (1996) 236–242, https://doi.org/10.1016/0925-8388(95)02136-1.
[59] L. Kaufman, Coupled thermochemical and phase diagram data for tantalum based binary alloys, Calphad 15 (1991) 243–259, https://doi.org/10.1016/0364-5916(91)90004-4.
[60] P.R. Subramanian, D.E. Laughlin, The Cu-Ta (Copper-Tantalum) system, Bulletin of Alloy Phase Diagrams 10 (1989) 652–655, https://doi.org/10.1007/BF02877637.
[61] L. Chen, N. Magtoto, B. Ekstrom, J. Kelber, Effect of surface impurities on the Cu/Ta interface, Thin Solid Films 376 (2000) 115–123, https://doi.org/10.1016/S0040-6090(00)01343-2.
[62] T. Qureshi, M.M. Khan, H.S. Pali, Review: high-entropy borides—Challenges and opportunities, J Mater Sci 59 (2024) 15921–15991, https://doi.org/10.1007/s10853-024-10064-1.
[63] Y. Mao, L. Peng, Q. Deng, D. Nie, S. Wang, L. Xi, Wetting behavior and interfacial interactions of molten Cu50Ti alloy with hexagonal BN and TiB2 ceramics, Ceram Int 42 (2016) 9906–9912, https://doi.org/10.1016/j.ceramint.2016.03.090.
[64] X.G. Song, Y. Lei, W. Fu, Z.K. Luo, H.L. Li, W.M. Long, S.P. Hu, Brazing of superhard AlMgB14–TiB2 ceramic to 304 stainless steel with AgCuTi filler alloy, Vacuum 197 (2022) 110810, https://doi.org/10.1016/j.vacuum.2021.110810.
[65] W. Yang, T. Lin, P. He, Y. Huang, J. Feng, Microstructural investigation of in situ TiB whiskers array reinforced ZrB2–SiC joint, J Alloys Compd 527 (2012) 117–121, https://doi.org/10.1016/j.jallcom.2012.03.016.